Earthq Eng & Eng Vib (2017) 16: 219-231 **DOI**:10.1007/s11803-017-0378-9

Spring tube braces for seismic isolation of buildings

V. Karayel[1†], E. Yuksel[2‡], T. Gokce[1†] and F. Sahin[2§]

1. *Institute of Science and Technology, Istanbul Technical University, Istanbul 34469, Turkey*

2. *Faculty of Civil Engineering, Istanbul Technical University, Maslak, Istanbul 34465, Turkey*

Abstract: A new low-cost seismic isolation system based on spring tube bracings has been proposed and studied at the Structural and Earthquake Engineering Laboratory of Istanbul Technical University. Multiple compression-type springs are positioned in a special cylindrical tube to obtain a symmetrical response in tension and compression-type axial loading. An isolation floor, which consists of pin-ended steel columns and spring tube bracings, is constructed at the foundation level or any intermediate level of the building. An experimental campaign with three stages was completed to evaluate the capability of the system. First, the behavior of the spring tubes subjected to axial displacement reversals with varying frequencies was determined. In the second phase, the isolation floor was assessed in the quasi-static tests. Finally, a ¼ scaled 3D steel frame was tested on the shake table using actual acceleration records. The transmitted acceleration to the floor levels is greatly diminished because of the isolation story, which effects longer period and higher damping. There are no stability and self-centering problems in the isolation floor.

Keywords: seismic isolation; spring tube; base isolation; low-cost isolation

1 Introduction

Two principal techniques to reduce building response during vibration are period shifting and addition of supplementary damping, (Makris and Chang, 2000; Yamada and Kobari, 2001). The period shifting technique significantly lengthens the fundamental period of the structure from the destructive frequency range of the vibration. The concept of base isolation as an application of the period shifting technique is now widely accepted in earthquake-prone areas of the world for protecting important structures from strong ground motions.

One of the historical concepts to lengthen the fundamental period of a building is to use a flexible first story (Kelly, 1986). In this concept, the columns of the first story are designed to have a much lower lateral stiffness than the columns above the first story. When the building is subjected to earthquake loading, the deformations are concentrated in these first-story columns. However, while the accelerations at the upper levels are reduced, the first-story columns have notably large displacements and the effect of the vertical load on this sideways movement of the column can produce severe damage to the columns; collapse of the building is a distinct possibility. In the modified version, which is called the soft first story method, the first-story columns yield during an earthquake, producing an energy-absorbing action and controlling the displacements (Fintel and Khan, 1969). However, to produce sufficient damping, the displacement must be large, and a yielded column has a significantly reduced buckling load. Thus, the instability and collapse of that column are inevitable (Chopra *et al*., 1973). Although the flexible first story method is no longer considered a strong candidate to decrease the accelerations in a building, it remains appealing to architects for esthetic reasons (Arnold, 1984).

Todorovska (1999) indicated that a soft story produced with inclined columns, which behaves as a physical pendulum, could be used as a seismic isolation system. The optimal inclination and its effectiveness depend on the frequency content of the excitation and can be evaluated for a scenario earthquake or using the probabilistic seismic hazard methodology. Comartin (2009) suggested supplemental vertical supports as a seismic retrofitting technique to eliminate the possibility of second-order effects of the existing columns in soft story type buildings. This suggestion indirectly indicates that the soft story can be assessed as an isolation story

Correspondence to: Ercan Yuksel, Istanbul Technical University Faculty of Civil Engineering Maslak Campus Maslak, Istanbul 34469, Turkey
Tel/Fax: +90 212 285 6761
E-mail: yukselerc@itu.edu.tr

†PhD Candidate; ‡Associate Professor; §Senior M.Sc. Structural Engineer

Supported by: Research Project 36997 of Istanbul Technical University Research Funds

Received May 23, 2015; **Accepted** October 11, 2015

when the second-order effects are eliminated. In the modern era, elastomeric bearings such as rubber-type bearings or lead-rubber-type bearings and frictional sliding systems are commonly used for seismic isolation (Skinner *et al*., 1993). Due to the relatively low damping property of natural rubber (LDRB), supplementary damping devices may also be used (Warn and Ryan, 2012). However, high damping rubber bearings (HDRB) have large displacement and damping capacities (Dezfuli and Alam, 2014) and they are one of the most economical and effective seismic isolators (Tsai *et al*., 2003). Calabrese (2013) developed a low-cost base isolation technology based on recycled rubber. Dynamic behaviour of buildings isolated with recycled rubber and fibre-reinforced bearings have been studied experimentally; the potential of low-cost and low quality elastomers has been shown.

It can be concluded from the chronological review that few studies directly practiced the soft story mechanism for vibration control of buildings. The main objective of this paper is to develop a new seismic isolation system based on the stable soft story mechanism for low-rise RC and steel buildings. The seismic isolation story, which is placed on the foundation level or any preferred intermediate level, consists of vertical hinged steel columns and diagonal spring tube braces. The gravitational loads are supported by the vertical columns, and the lateral stability of the system is mainly governed by the diagonal spring tube bracings. The column end hinges are connected to the rigid upper and lower floor beams. The seismic isolation story, which has relatively low lateral stiffness, lengthens the fundamental vibration periods of the building, which significantly decreases the lateral accelerations to be transmitted to the upper stories of the building. Thus, the plastic energy demands and input seismic energy of the building substantially decrease.

Prior to the experimental works, an analytical study with time history analyses of the three-story ¼ scale test frame and its fixed-base version was accomplished. The structural response parameters obtained from the models, such as the base shear, acceleration, velocity and displacements at the story levels and the inter-story drifts, were compared (Karayel and Yuksel, 2013).

The foremost advantages of the proposal against the existing base isolation systems are as follows:

(1) There is no requirement to add a service story to the building. The seismic isolation story can be used for consistent purposes.

(2) The members of the seismic isolation story, i.e., the steel columns and spring tube braces, can be produced by local and low-profile workmanship.

(3) The maintenance and replacement of members of the seismic isolation story are relatively easy.

(4) The cost is reasonably low.

The completed experimental studies proved that the proposed seismic isolation story helped to solve great displacement demands and second-order effects. The self-centering capability (Medeot, 2012) and the system's own fail-safe mechanism (Kelly and Beucke, 1983; Ohari *et al*., 1988) were observed.

2 Spring tube braces

The seismic isolation system consists of steel columns with pinned connections at both ends and spring tube braces. Each spring tube has a steel cylindrical web and two end pistons. Four identical linear elastic helical compression springs with stiffness (k) are positioned in the spring tube. When the spring tube is subjected to tension force, the external helical springs are compressed. When the spring tube is subjected to compression forces, the internal springs are compressed. The longitudinal section of the spring tube is illustrated in Fig. 1.

The main physical properties of the helical compression springs in this study, i.e., the wire diameter, outer and mean diameter of the coil, free length and number of active coils, are shown in Fig. 2. The ground-type ends of the springs enable continuous touching to the flat surface of the pistons.

The axial stiffness of the spring tube (K) is equivalent to half of the stiffness (k) of an identical helical compression spring (Eq. (1)).

$$\begin{aligned} P &= K\times 2\Delta \\ k &= P/\Delta \\ K &= k/2 \end{aligned} \tag{1}$$

3 Seismic isolation story

The seismic isolation story, which is implemented on the foundation level or any intermediate level of the

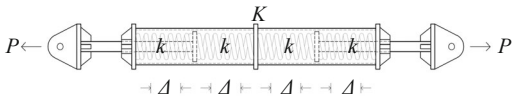

Fig. 1 Typical longitudinal section of the spring tube

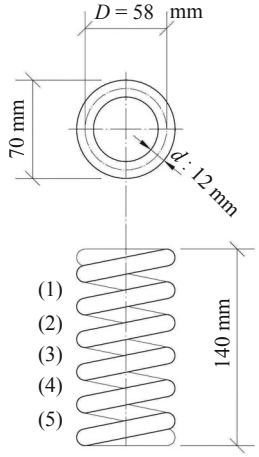

Fig. 2 Properties of the helical compression spring

building, consists of pinned-end steel columns and spring tube braces. The steel columns with hinges at both ends are connected to the rigid beams. The lateral stiffness of the seismic isolation story is governed by the spring tube braces. The first- and second-order lateral stiffness values of the seismic isolation story are calculated for the system in Fig. 3.

The lateral stiffness of the seismic isolation story (K_x) is calculated considering the axial stiffness of the spring tube (K) and the inclination angle (α) (Eq. (2)). The second-order lateral stiffness is determined from Eq. (3) or Eq. (4), where the (N/h) ratio represents the second-order effect of the vertical loading (Wilson and Habibullah, 1987).

$$K_x^{\mathrm{I}} = K \times \cos^2\alpha \tag{2}$$

$$K_x^{\mathrm{II}} = K \times \cos^2\alpha - (N/h) \tag{3}$$

$$K_x^{\mathrm{II}} = K_x^{\mathrm{I}} - (N/h) \tag{4}$$

The first- and second-order lateral stiffness of the story can also be defined by simply inverting the corresponding lateral displacement Δ (Eq. (5) and Fig. 3).

$$K_x = 1/\Delta \tag{5}$$

The geometrical compatibility equations of the seismic isolation story are determined as follows. The length of the spring tube and the distance between two pins of the tube are denoted by a and b, respectively (Fig. 4).

The changes in diagonal lengths (Δd and Δp) and vertical settlement (Δy) are determined in the distinct lines of Fig. 5 for pulling- and pushing-type loadings.

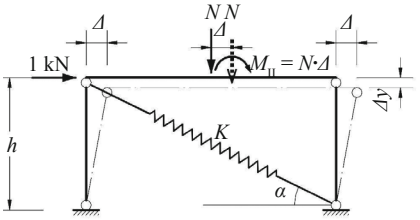

Fig. 3 Deformed shape of the seismic isolation story because of a unit lateral force

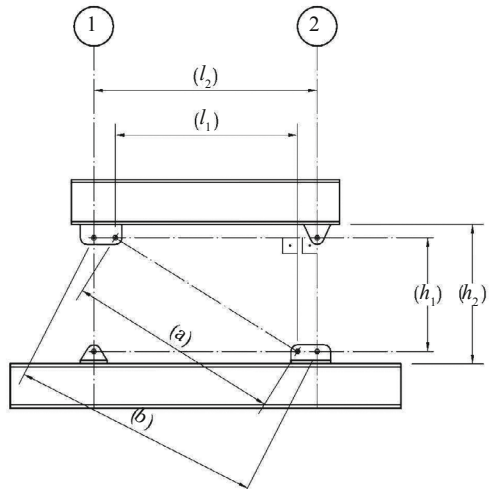

Fig. 4 Undeformed shape of the seismic isolation story and related parameters

4 Experimental studies

Experimental works were performed in three successive stages to determine the competence of the spring tube braces for the seismic isolation of low-rise buildings: uniaxial loading tests of the spring tubes, quasi-static tests of the seismic isolation story and shake table tests of a 3-story ¼ scale model structure with a seismic isolation story. Details are presented in the following paragraphs.

4.1 Uniaxial loading test of the spring tube

The test aims to determine the axial stiffness of the spring tube and evaluates the success of the analytical equation, Eq. (1). The dimensions of the tested spring tube are shown in Fig. 6(a). The spring tube is connected to the testing setup by simple hinges at both ends (Fig. 6(b)). Reverse displacement cycles were applied to the specimen using a servo controlled MTS actuator present in the Structural and Earthquake Engineering Laboratory of Istanbul Technical University. The force-displacement relation that was obtained from the tests is in the linear elastic form (Fig. 6(c)). The determined stiffness of the spring tube is K = 110 kN/m, which is equal to half of the stiffness of one helical compression spring: K = 220 kN/m (see Eq. (1)). The experimental response of the spring tube is exactly identical for tension and compression directions. No indication is observed for the gap on the response curves.

4.2 Quasi-static tests of the seismic isolation story

The performance of the seismic isolation story was examined using quasi-static tests in the laboratory. First and second order lateral stiffness, axial forces in the members are obtained and the verification of geometrical compatibility equations is achieved from the tests.

The general dimensions of the control story are shown in Fig. 7. The inclination angle α of the spring tube is 32°. The distance between two pins of the columns (h) is 510 mm. The exterior diameter of the pipe-type columns is 88.9 mm, and the thickness is 4 mm.

The test setup that represented the seismic isolation story had two identical frames, which were connected to each other by rigid steel beams (Fig. 8(a)). The servo controlled DARTEC actuator was fastened to the test specimen to apply the target displacement pattern. The vertical columns and spring tubes were connected to the rigid beams using simple hinges. The washers and nuts of the hinged connections are removed to minimize the frictional effects. The damping potential of the hinged connection was sacrificed in the quasi-static tests to

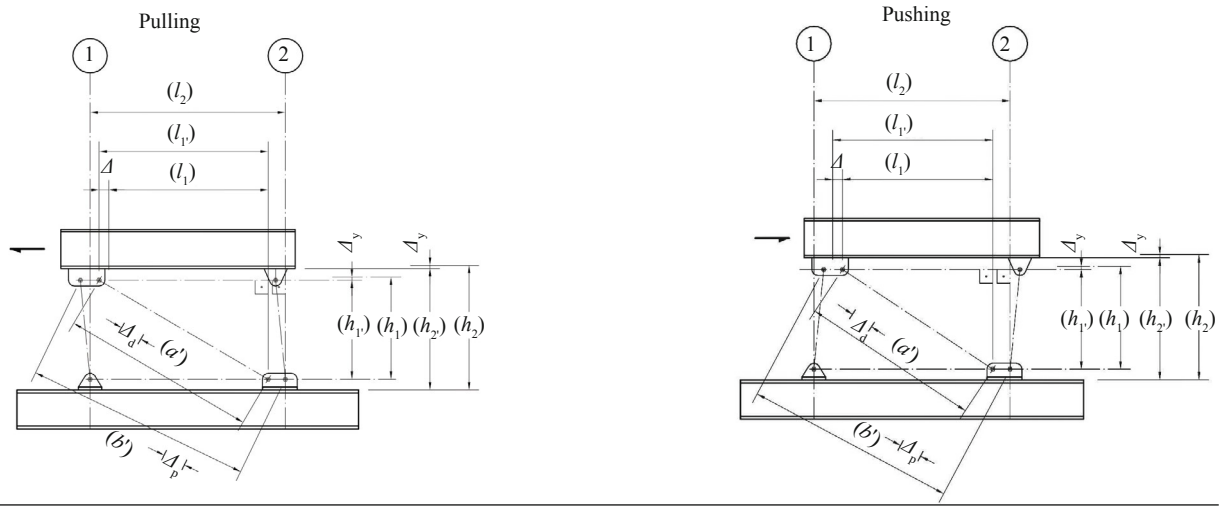

$$l_{1'} = l_1 + \Delta \qquad l_{1'} = l_1 - \Delta$$

$$a' = \sqrt{\left[(h_1')^2 + (l_1')^2\right]}$$

$$\Delta_d = a' - a$$

$$b' = \sqrt{\left[(h')^2 + (l_2 + \Delta)^2\right]} \qquad b' = \sqrt{\left[(h')^2 + (l_2 - \Delta)^2\right]}$$

$$\Delta_p = b' - b$$

$$\Delta_y = h_1 - h_{1'} \text{ and } \Delta_y = h_2 - h_{2'},$$

Fig. 5 Geometrical compatibility equations of the seismic isolation story

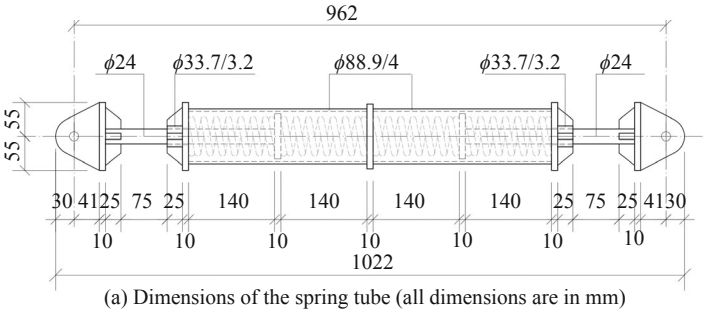

(a) Dimensions of the spring tube (all dimensions are in mm)

(b) Testing setup

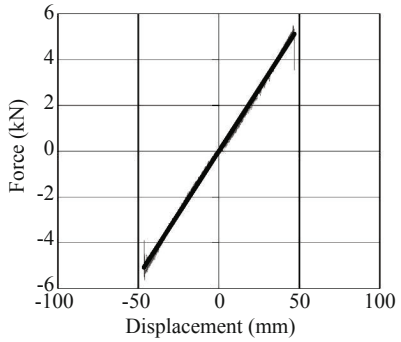

(c) Force displacement relation

Fig. 6 Uniaxial loading test of the spring tube

make possible comparison with the analytical results given in Section 3.

The test specimen was rigidly connected to the testing frame. Several strain gauges and displacement transducers were placed at different positions on the test specimen (Fig. 8). Steel plates were used to simulate the vertical loads on the seismic isolation story. Four distinct vertical load intensities were used in the study: 0 kN, 5.0 kN, 25.0 kN and 30.5 kN. Cyclic displacement reversals were applied to the specimen. Displacement increments are selected as 5 mm and each displacement target was repeated one time.

The test specimen is colored with green, and the diagonal spring tubes are colored with yellow (Fig. 9)

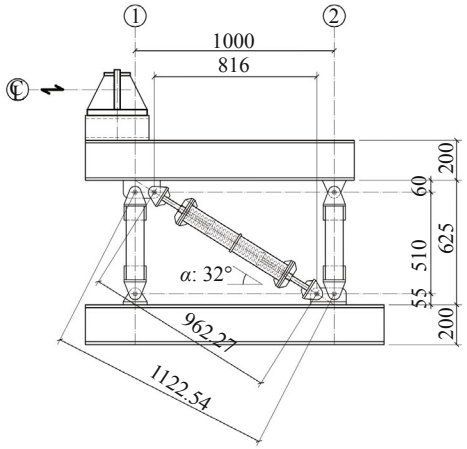

Fig. 7 Geometry of the seismic isolation story (all dimensions are in mm)

in the test setup.

The general response of the seismic isolation story is linear elastic for discrete vertical loading states (Fig. 10). No residual displacement was recorded at the end of the tests. The slope of the force vs. displacement relations in Fig. 10 decreases with increasing vertical load intensity. The slopes are 0.1545 kN/mm, 0.1400 kN/mm, 0.0993 kN/mm and 0.0904 kN/mm for the vertical load intensities of 0 kN, 5.0 kN, 25.0 kN and 30.5 kN, respectively. The decrease is attributed to the second-order effects of vertical loading.

For distinct vertical load intensities, the experimentally obtained lateral stiffness values of the seismic isolation story were compared with the analytical results, where the story height is 510 mm, which corresponds to the distance between both end pins of the columns. The minimum and maximum relative

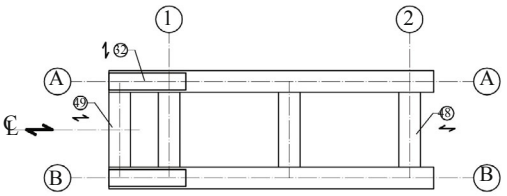

Squared and circled numbers in figures stand for strain gauges and displacement transducers.

(a) Plan view of the specimen

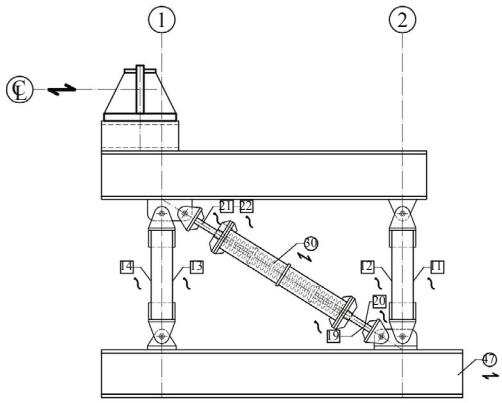

(b) Elevation of the B axis

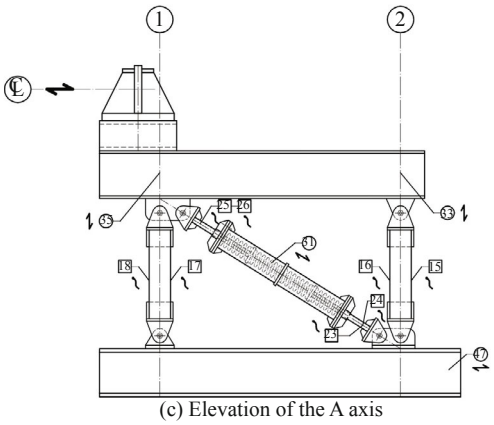

(c) Elevation of the A axis

Fig. 8 Deformation and displacement measuring systems

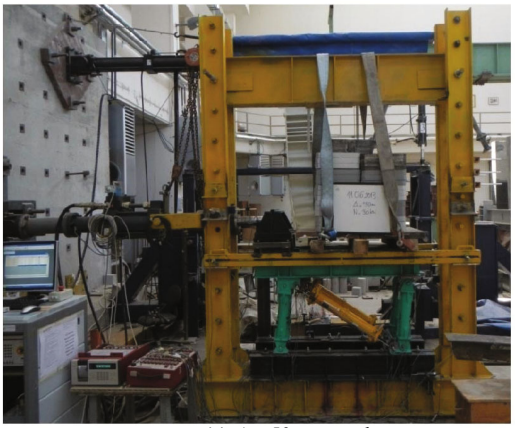

(a) Δ = 50 mm push

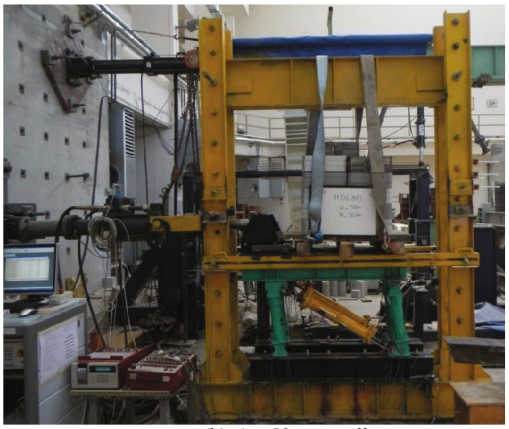

(b) Δ = 50 mm pull

Fig. 9 Quasi-static testing with 30 kN vertical loading

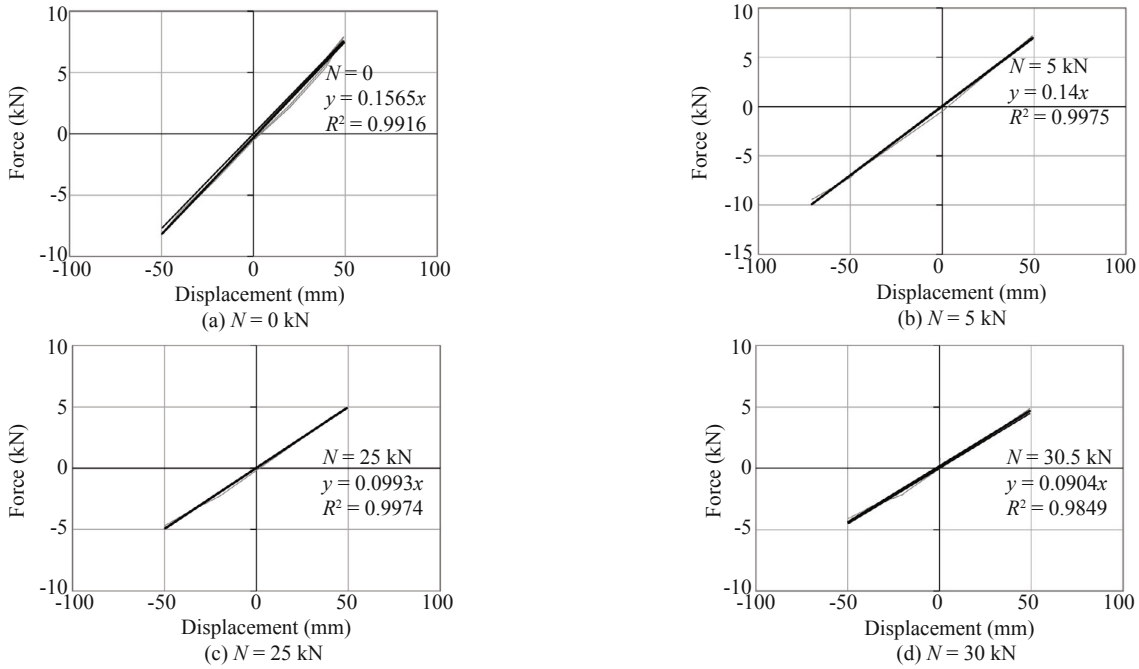

Fig. 10 Force displacement relations of the seismic isolation story

Table 1 Comparison of the experimentally and analytically obtained lateral stiffness values

N (kN)	Experimental	Analytical	Relative difference (%)
	$K_x = P/\Delta$ (kN/m)	$K_x = K\cos^2\alpha - N/h$ (kN/m)	
(1)	(2)	(3)	(4)
0	157.0	158.2	0.8
5.0	140.0	148.4	6.0
25.0	100.0	109.2	9.2
30.5	91.0	98.3	8.0

differences between the experimental and analytical results are 0.8% and 9.2%, respectively (column (4) of Table 1).

In the experimental study, the measured diagonal and vertical displacements of two frames are shown in Columns (2), (3) and (4) of Table 2. For each lateral displacement step, the corresponding diagonal and vertical displacements were calculated from the derived compatibility equations and are shown in Columns (5) and (6) of Table 2. The analytical results are practically close to the corresponding experimental results.

For one of the force vs. displacement pairs in Columns (1) and (2) of Table 3, more comprehensive analyses were accomplished to verify the experimental results. The lateral stiffness, which was calculated from the force to displacement ratio, is $k_x = P/\Delta = 93.21$ kN/m. The corresponding spring tube force is determined from Eq. (1) and is shown in Column (4) of Table 3. The force that corresponds to one spring tube was determined by simply dividing the F force by 2 and is shown in Column (5) of Table 3. The strains, which were measured using strain gauges at different sections of the spring tube's stroke, are listed in Column (7) of Table 3, and their averages are shown in Column (8). The axial stress on the stroke was calculated by multiplying the average strain by the Young modulus. Hence, the axial force of the spring tube was calculated by multiplying the average stress by the cross-sectional area of $A = 179$ mm^2. The calculated spring tube forces (Column (10)) are consistent with the calculated forces in Column (5).

For the second verification, the displacement that was measured, the displacement transducers on the stroke of the spring tube and the axial stiffness of the tube were used. The average displacements measured on the spring tubes are $\Delta_d = 43.0$ mm for the lateral displacement of 49.85 mm (Column (1) of Table 3). The calculated lateral stiffness of the seismic isolation story is $k_x = 93.21$ kN/m. The cumulative axial stiffness of the spring tubes can be obtained from the lateral stiffness as $k = k_x/\cos^2\alpha = 129.60$ kN/m. Half of this value, which is 64.8 kN/m, corresponds to the axial stiffness of one spring tube. Hence, the axial stiffness was multiplied by the displacement to obtain the axial force of the spring tube as $64.8\text{kN/m}\times 43\times 10^{-3}$ m = 2.78 kN, which is also similar to the forces in Columns (5) and (10) of Table 3.

For the final verification, the diagonal displacement $\Delta_d = 43.24$ mm, which was calculated from the geometrical compatibility equations in Fig. 5 and the axial stiffness of 98.3 kN/m, was used (Column (3) of Table 1). The lateral stiffness of each spring tube is $k_x =$

Table 2 Displacements of the seismic isolation story

Lateral disp. measured in actuator stroke	Experimental results		Analytical results		
	Diagonal disp. of Frame a	Diagonal disp. of Frame b	Vertical disp. (downward)	Diagonal disp. Δ_d	Vertical disp. Δ_y
(1)	(2)	(3)	(4)	(5)	(6)
(mm)	(mm)	(mm)	(mm)	(mm)	(mm)
19.67	-15.30	-15.38	0.26	-16.83	0.38
39.34	-32.68	-33.28	1.30	-33.96	1.52
49.17	-41.80	-42.24	2.00	-42.64	2.37
39.34	-34.28	-33.66	1.30	-33.96	1.52
19.67	-16.94	-16.44	0.26	-16.83	0.38
-19.80	12.02	15.20	0.44	16.65	0.38
-39.68	28.38	31.10	1.75	33.08	1.55
-49.62	37.12	39.48	2.66	41.20	2.42
-39.67	31.00	33.40	1.73	33.07	1.55

Table 3 Spring tube forces for N = 30.5 kN vertical loading

Δ	P	$k_x = P/\Delta$	$F = P/\cos\alpha$	$F_1 = F/2$	Spring tube	ε	$\varepsilon_{average}$	$\sigma = \varepsilon \cdot E$	$F = \sigma \cdot A$
(1)	(2)	(3)	(4)	(5)	(6)	(7)	(8)	(9)	(10)
(mm)	(kN)	(kN/m)	(kN)	(kN)		mμ	mμ	(kN/m^2)	(kN)
49.85	-4.65	93.21	-5.48	-2.74	1	15	-79	-16600	-2.97
						-173			
						-43	-70	-14800	-2.64
						-97			
					2	-194	-75	-15600	-2.79
						45			
						-54	-78	-16400	-2.92
						-101			

49.15 kN/m, so the corresponding axial stiffness is $k = k_x/\cos^2\alpha$ = 68.35 kN/m. The axial force of the spring tube was calculated as the product of these values: 68.35 kN/m × 43.24×10^{-3} m = 2.95 kN, which is fairly similar to the experimental values in columns (5) and (10) of Table 3.

Consequently, the lateral stiffness of the seismic isolation story, which is notably effective on the dynamic behavior, can be estimated using the proposed equations.

4.3 Shake table tests

The effectiveness of the seismic isolation system was examined using a series of dynamic tests on the shake table. The ¼ scale one-bay three-story steel moment-resisting frame was used as the test specimen (Fig. 11). The span length in two directions is 1 m, and the story heights are 0.75 m. Modelling rules were used to determine the structural properties (Noor and Boswell., 1992), Table 4. The in-plane stiffness of the floors was provided by the secondary beam system. The sectional properties of the box-type columns and primary and secondary beams of the superstructure and the specimen geometry are shown in Figs. 11(a) and 11(b). The seismic isolation story is identical to the specimen in the quasi-static tests. However the hinged connections of the isolated story columns are partially fixed by means of the nuts and washers.

Because the tests were performed on a uni-axial shaking table, the out-of-plane stability of the 3D test frame was formed using the vertical bracings on the axes of 1 and 2 (Fig. 11(a)). A section of the bracings was selected as thin plates to eradicate the flexural rigidity in the loading direction.

Sensebox-3D accelerometers with ±2 g measuring capacity were placed on the floor level for the specimen and the shake table. The accelerometers are shown as diamond shapes in Fig. 11(c). The lateral displacements were also measured at the level of the shake table, on top of the isolation story and on top of the specimen. The potentiometric rulers with different stroke capacities were fixed to the same reference frame (Fig. 11(c)). The positions of the rulers are shown as circled numbers in Fig. 11(c). The mass intensities, which are defined according to the similitude laws, are 1.38 and 1.04 kNs^2/m for the seismic isolation story and the upper floors, respectively. The masses were rigidly fixed to the secondary beams in

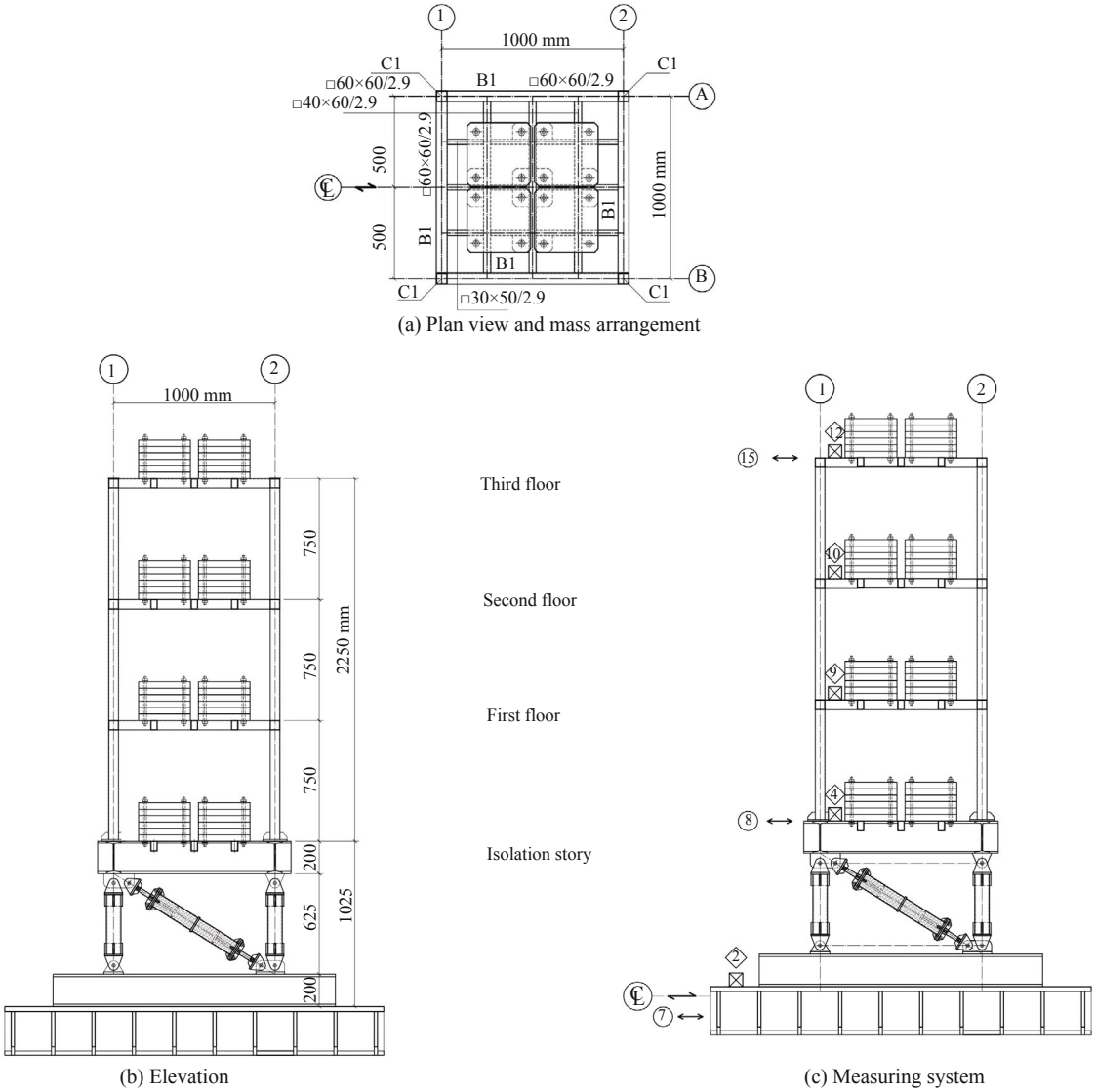

(a) Plan view and mass arrangement

(b) Elevation

(c) Measuring system

Fig. 11 Test specimen and the measuring system

the floor system (Fig. 11). The modal characteristics of the tested specimen were determined using FFT analyses of the acceleration data that were recorded on the seismic isolation story (Fig. 12). The dominant frequencies are f_1 = 0.56 Hz and f_2 = 5.34 Hz, which correspond to the first and second vibrational modes. The vibrational mode shapes that were generated from the experimental data are shown in Fig. 13.

The first vibrational frequency can be readily determined by assuming a single degree of freedom system (Eq. (6)).

$$T_1 = 2\pi\sqrt{\frac{m}{K_x^{\mathrm{II}}}} \tag{6}$$

The lateral stiffness of the seismic isolation story is calculated from Eq. (3) as follows.

$K_x^{\mathrm{II}} = K \times \cos^2\alpha - (N/h) = 220 \times 0.719 - (49.8/0.51) =$ 60.53 kN/m

where N corresponds to the total weight on the isolation story, which includes the supplementary masses and self-weight of the specimen as N = 13.8 + 10.4 × 3 + 4.8 = 49.8 kN. The other parameters (K, α and h) are determined above.

The frequency is calculated using Eq. (6).

$$T_1 = 2\pi\sqrt{\frac{4.98}{60.53}} = 1.80 \text{ s}$$

$$f_1 = 1/T_1 = 0.56 \text{ Hz}$$

The analytically calculated frequency is consistent with the experimental result (Fig. 13).

The free vibration tests were consecutively repeated on the specimen, and the results of successive measurements did not change. Hence, the stiffness properties of the vibration isolation story did not change during the entire experimental campaign.

The acceleration records in the experimental study

Table 4 Scaling factors for the various quantities

Constant	Symbol	Relation	Scale factor
Dimension	l	λ_l	4.0
Modules of elasticity	E	λ_E	1.0
Acceleration	a	$\lambda_a = \lambda/\lambda_1\lambda_E/\lambda_\rho$	1.0
Velocity	v	$\lambda_v = (\lambda_l \lambda_a)^{1/2}$	2.0
Force	F	$\lambda_f = \lambda_E\lambda_l^2$	16.0
Stress	σ	$\lambda_\sigma = \lambda_E$	1.0
Strain	ε	$\lambda_\varepsilon = 1.0$	1.0
Area	A	$\lambda_A = \lambda_l^2$	16.0
Volume	V	$\lambda_v = \lambda_l^3$	64.0
Moment of inertia	I	$\lambda_I = \lambda_l^4$	256.0
Density	ρ	$\lambda_\rho = \lambda_E/(\lambda_l\lambda_a)$	0.25
Mass	m	$\lambda_m = \lambda_\rho\lambda_l^3$	16.0
Momentum	i	$\lambda_i = \lambda_l^3/(\lambda_l \lambda_a)^{1/2}$	32.0
Energy	e	$\lambda_e = \lambda_E\lambda_l^3$	64.0
Time	t	$\lambda_t = (\lambda_l /\lambda_a)^{1/2}$	2.0
Frequency	ω	$\lambda_\omega = 1/\lambda_l(\lambda_E /\lambda_\rho)^{1/2}$	0.5
Ground acc.	g	$\lambda_g = 1.0$	1.0
Ground force	f_g	$\lambda_{fg} = \lambda_\rho\lambda_l^3$	16.0
Damping	ζ	$\lambda_\zeta = 1.0$	1.0

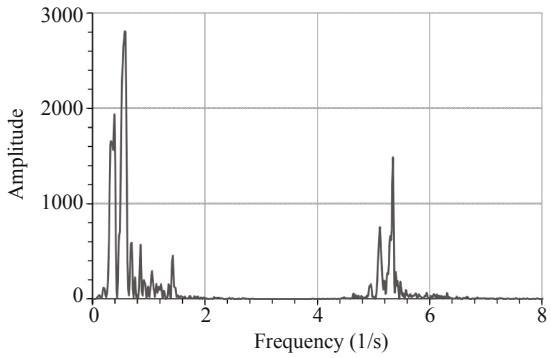

Fig. 12 FFT analyses of the recorded data

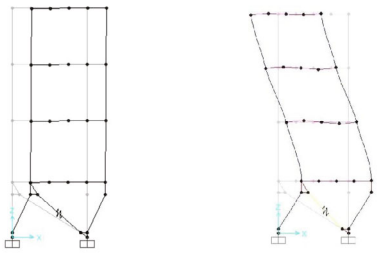

Fig. 13 First two vibrational mode shapes

are shown in Table 5. The PGA and PGV parameters of the records are shown in the last two columns of the table. Period vs. elastic spectral acceleration curves of the selected records and the code-specified design spectra for firm- and weak-type soils according to TEC (2007) are also shown in Fig. 14.

Photographs of the seismic isolation story and test specimen on the shake table are shown in Fig. 15.

For seven earthquakes, the recorded accelerations at the control story level are shown with the acceleration recorded on the shake table (Fig. 16). The recorded accelerations at the bottom and top of the control story

Table 5 Selected acceleration records

Record	Symbol	M_s	d (km)	PGA (cm/s^2)	PGV (cm/s)
Erzincan 03/13/1992 Erzincan S.	ERZ-EW	6.90	8.97	486.6	64.3
Superstition Hills 11/24/1987 USGS 5051 P. Test Site S.	PTS315	6.60	15.99	369.8	43.9
Chi-Chi, Taiwan 09/20/1999 CWB 99999 TCU076 S.	TCU076	7.62	16.03	408.1	64.2
Chi-Chi, Taiwan 09/20/1999 CWB 99999 TCU067 S.	TCU067	7.62	28.70	318.8	66.6
Loma Prieta 10/18/1989 Hollister Diff. Array S.	HDA165	7.10	45.10	263.9	43.9
Superstition Hills 11/24/1987 USGS 9400 Poe Road S.	POE360	6.60	11.20	294.3	32.8
Duzce 12/11/1999 Bolu S.	BOL000	7.14	17.16	714.2	56.4

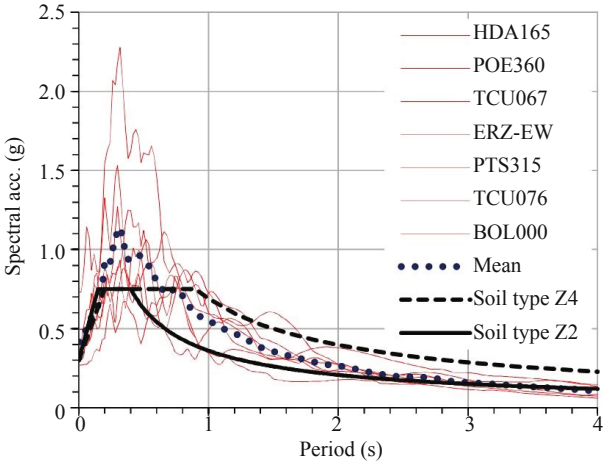

Fig. 14 Elastic spectral accelerations

are substantially different in terms of intensity and frequency.

The target and measured accelerations on the shake table are shown in the 2nd and 3rd columns of Table 6, respectively. The maximum observed accelerations of the floor levels are shown in Columns (4), (5), (6) and (7) of Table 6. In addition, the recorded acceleration intensities of the story levels are principally lower than the shake table acceleration.

The ratios between the floor and shake table accelerations are shown in Table 7. The obtained acceleration ratios are 0.17–0.54. The average acceleration ratio above the isolation story is 0.32, which indicates that the acceleration intensity decreases by 68%.

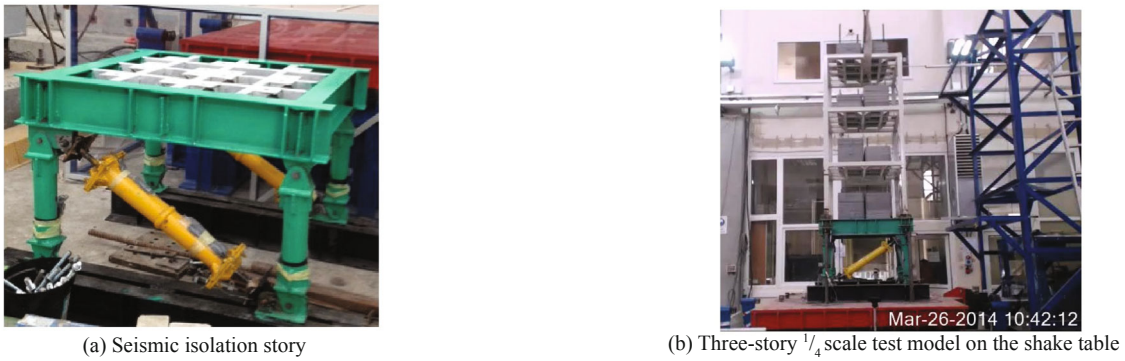

(a) Seismic isolation story (b) Three-story $^{1}/_{4}$ scale test model on the shake table

Fig. 15 Seismic isolation story and test specimen

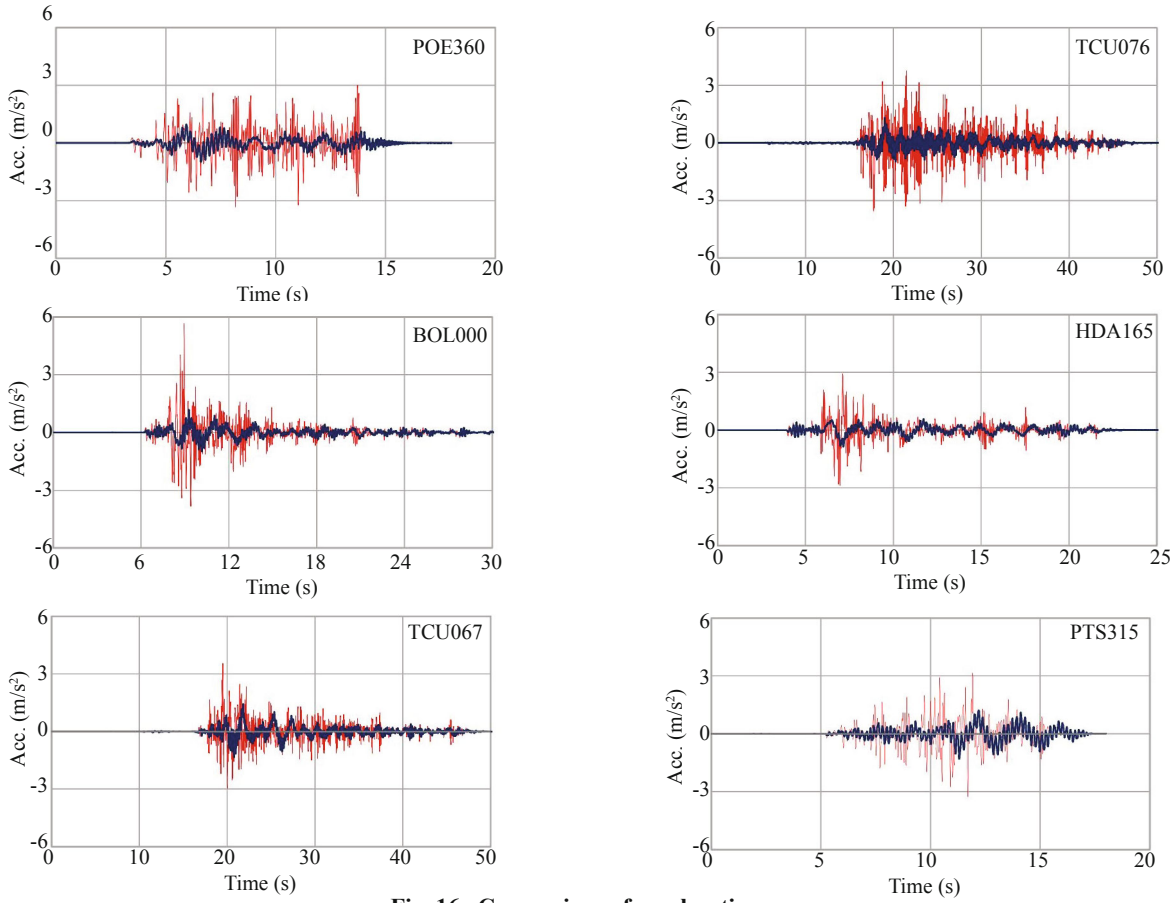

Fig. 16 Comparison of accelerations

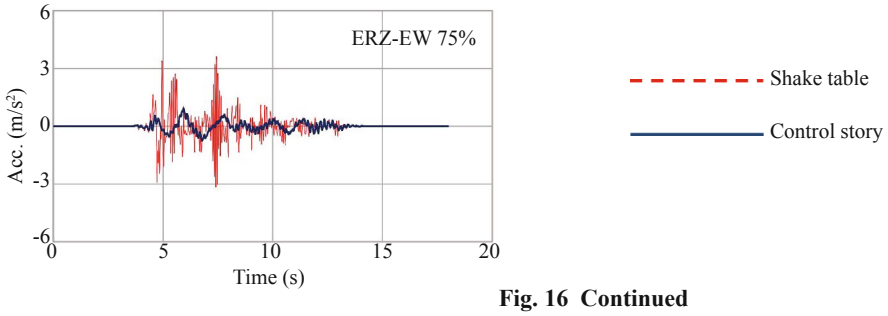

Fig. 16 Continued

Table 6 Recorded maximum accelerations

Earthquake	Target acc. (m/s²)	Acc. measured on shake table (m/s²)	Isolation story (m/s²)	First floor (m/s²)	Second floor (m/s²)	Third floor (m/s²)
(1)	(2)	(3)	(4)	(5)	(6)	(7)
POE360	2.946	3.320	0.981	0.827	0.840	1.170
TCU076	4.079	3.768	1.329	1.171	1.356	1.637
BOLU	7.138	5.663	1.181	0.971	1.055	1.600
HDA165	2.636	2.920	0.859	0.822	0.914	1.112
TCU067	3.192	3.539	1.435	1.371	1.534	1.916
PTS315	3.700	3.272	1.276	1.181	1.176	1.642
ERZ-EW 75%	3.646	3.623	0.935	0.951	0.983	1.084

Table 7 Acceleration ratios

Earthquake	Shake table	Control story	First floor	Second floor	Third floor
POE360	1.00	0.30	0.25	0.25	0.35
TCU076	1.00	0.35	0.31	0.36	0.44
BOLU	1.00	0.21	0.17	0.19	0.29
HDA165	1.00	0.29	0.29	0.31	0.38
TCU067	1.00	0.41	0.39	0.43	0.54
PTS315	1.00	0.39	0.36	0.36	0.50
ERZ-EW 75%	1.00	0.26	0.26	0.27	0.30
Average		0.32	0.29	0.31	0.40
Standard deviation		0.07	0.07	0.08	0.10
CoV		0.22	0.24	0.26	0.25

The relative accelerations between consecutive floors of the test specimen are shown in Table 8. The values are much smaller than the analytically obtained values from the fixed-based version of the specimen, (Karayel and Yuksel, 2013). Hence, the possibility of structural damage is strictly decreased.

The relative lateral displacement of the seismic isolation story for each acceleration record is presented in Table 9. The minimum and maximum relative displacements are 46.86 mm and 85.84 mm, respectively. The corresponding drift ratios are also presented in Table 9. The drifts are 9.19%–16.83%. The observed maximum displacement at the axis of the spring tubes is 75.77 mm, which is smaller than its displacement capacity.

Residual displacements were not observed at the isolation story after the entire test campaign was completed. Thus, there is no self-centering problem for the specimen.

If the displacement demand exceeds the capacity of the isolation story, the springs in the tubes lose their

Table 8 Relative accelerations between floors

Earthquake	First floor (m/s²)	Second floor (m/s²)	Third floor (m/s²)
POE360	-0.154	0.013	0.330
TCU076	-0.158	0.185	0.281
BOLU	-0.210	0.084	0.545
HDA165	-0.037	0.092	0.198
TCU067	-0.064	0.163	0.382
PTS315	-0.095	-0.005	0.466
ERZ-EW 75%	0.016	0.032	0.101

Table 9 Relative displacements and drifts of the isolation story

Earthquake	Relative displacement (mm)	Drift (%)
POE360	51.61	10.12
TCU076	68.57	13.45
BOLU	46.86	9.19
HDA165	69.62	13.65
TCU067	85.84	16.83
PTS315	60.65	11.89
ERZ-EW 75%	60.00	11.76

functionalities, so the system becomes comparatively stiffer because of the entirely closed or opened rigid pistons of the spring tubes. Because the isolation story has this instantaneous increase in lateral stiffness, the accelerations that are transmitted to the upper part are relatively increased, but the overall stability of the system is endangered. Therefore, the fail-safe mechanism is generated by the system. This phenomenon was experienced when 100% of the ERZ-EW record was applied. Thus, the scaling factor of 75% was selected for the ERZ-EW record, see Table 6.

In a companion study which has just been completed (Karayel *et al*., 2015), it was observed that large structural damping arose from the 'hinged' beam to column connections in the isolation story due to the friction on the pinned connections of the columns to beams and spring tubes. Hereafter, the energy balance methodology (Akiyama, 1985) was applied to the shake table test results, Eq. (7).

$$\int \boldsymbol{m}\ddot{\boldsymbol{u}}(t)\dot{\boldsymbol{u}}(t)\mathrm{d}t + \int \boldsymbol{c}\dot{\boldsymbol{u}}(t)\dot{\boldsymbol{u}}(t)\mathrm{d}t + \int \boldsymbol{f}_s\dot{\boldsymbol{u}}(t)\mathrm{d}t = -\int \boldsymbol{m}\ddot{\boldsymbol{u}}_g(t)\dot{\boldsymbol{u}}(t)\mathrm{d}t \tag{7}$$

where $\boldsymbol{m}$, $\boldsymbol{c}$ and $\boldsymbol{f}_s$ are mass, damping and restoring force matrices, respectively, $\ddot{\boldsymbol{u}}$ and $\dot{\boldsymbol{u}}$ are relative acceleration and relative velocity and $\ddot{\boldsymbol{u}}_g$ is ground acceleration. Damping matrix $\boldsymbol{c}$ can be written in the following form Eq. (8),

$$\boldsymbol{c} = 2\xi\omega\boldsymbol{m} \tag{8}$$

where ξ is the critical damping ratio and ω is the circular frequency, if Eq. (7) is reformed as follows:

$$E_K + E_D + E_S = E_I \tag{9}$$

The terms on the left hand side of Eq. (9) represent the energy components of the structure, namely, kinetic (E_K), damping (E_D) and strain (E_S) energies. The right-hand side refers to the total input energy (E_I) imposed on the structure.

The graphical representation of the energy balance for the base isolated specimen for Superstition Hills POE360 EQ is illustrated in Fig. 17. Equivalent damping is determined about 18%–20% for POE360 similar to other EQs. This relatively high damping property can be attributed to the friction on the pinned connections of the columns to beams and spring tubes. The responses of the base isolated and fixed base specimens are also compared in (Karayel *et al*., 2015).

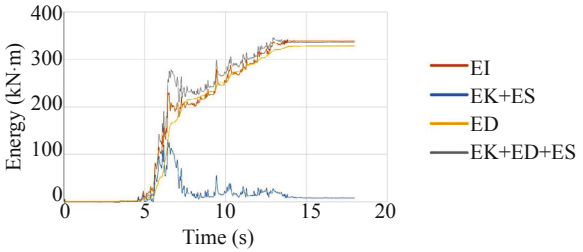

Fig. 17 The energy balance graphic for the experimental results

5 Conclusions

This study investigates the effectiveness of the new seismic isolation system based on spring tube bracings. The general conclusions are:

- Static tests performed on the spring tubes show that the analytical and experimental axial stiffness values of the spring tube are consistent.
- Quasi-static tests performed on the seismic isolation story are consistent with the analytical results in terms of the first- and second-order lateral stiffness, lateral and vertical displacements and internal forces on the spring tube.
- The proposed seismic isolation system is notably effective in reducing the intensity of accelerations.
- In the isolated structure, the floor accelerations and their differences are small compared to the ordinary fixed-based structures, which moves the structure away from the destructive range.
- The maximum observed drift of the seismic isolation story is approximately 16%, which is sufficiently large to withstand the demands of the design earthquake.
- Relatively high damping ratio of 18%–20% is obtained because of the friction in the partially fixed 'hinged' connections of the base isolation story columns.
- The self-centering capability was experienced during the shake table tests.
- When the ultimate displacement capacity of the spring tube is exceeded, the seismic isolation story has its own fail-safe mechanism.

The shake table tests are ongoing to evaluate the effectiveness of the proposed base isolation system. The analytical study is also progressing on a five story RC building. In a succeeding research project, it is planned to perform shake table tests for a full scale RC prototype having some proper engineering details. It is clear that all of these stages should be accomplished and satisfactory results obtained prior to engineering implementation.

Acknowledgment

This study was conducted in the Structural and Earthquake Engineering Laboratory of Istanbul Technical University. It was sponsored by research project 36997 of Istanbul Technical University Research Funds.

References

Akiyama H (1985), *Earthquake-resistant Limit-state Design for Buildings*, University of Tokyo Press, ISBN 0-86008-377-2.

Arnold C (1984), "Soft First Stories: Truths & Myths," *8th Word Conference on Earthquake Engineering*, San Francisco, **5**: 943–950.

Calabrese A (2013), "Analytical, Numerical and Experimental Study of a Novel Low-cost Base Isolation System," *PhD Thesis*, Submitted to University of Naples, "Federico II", 227 Pages.

Chopra AK, Clough DP and Clough RW (1973), "Earthquake Resistance of Buildings with a Soft First Storey," *International Journal of Earthquake Engineering and Structural Dynamics*, **1**: 347–355.

Comartin CD (2009), Supplemental Vertical Support as a Means for Seismic Retrofit of Buildings, *Seismic Risk Assessment and Retrofitting with Special Emphasis on Existing Low Rise Structures*, Editors: Ilki, A., Karadogan, F., Pala, S., Yuksel, E., Chapter 16, pp. 329–342, Springer.

Dezfuli FH and Alam MS (2014), "Sensitivity Analysis of Carbon Fiber-reinforced Elastomeric Isolators Based on Experimental Tests and Finite Element Simulations," *Bulletin of Earthquake Engineering*, **12**: 1025–1043.

Fintel M and Khan RF (1969), "Shock Absorbing Soft Story Concept for Multistory Earthquake Structures," *Journal of the American Concrete Institute*, **66**(29): 318–390.

Karayel V and Yuksel E (2013), "A New Seismic Base Isolation System Using Spring Tube Bracings," *International Conference on Earthquake Engineering*, Paper No: 222, Skopje, Macedonia.

Karayel V, Yuksel E, Gokce T and Sahin F (2015), "Uni-axial Shaking Table Tests and Validations of a Seismic Isolation System Made of Spring Tube Braces," under Review.

Kelly JM (1986), "Aseismic Base Isolation: Review and Bibliography," *Soil Dynamics and Earthquake Engineering*, **5**(3): 202–216.

Kelly JM and Beucke KE (1983), "A Friction Damped Base Isolation System with Fail-safe Characteristics," *Earthquake Engineering and Structural Dynamics*, **11**: 33–56.

Makris N and Chang S (2000), "Effect of Viscous, Viscoplastic and Friction Damping on the Response of Seismic Isolated Structures," *Earthquake Engineering and Structural Dynamics*, **29**: 85–107.

Medeot R (2012), "Re-centering Capability of Seismic Isolation Systems: A Controversial Matter Moving Scarcely Towards Its Settlement," *15th Word Conference on Earthquake Engineering*, Lisbon.

Noor FA and Boswell LF (1992), *Small Scale Modeling of Concrete Structures*, Elsevier Science Publisher Ltd.

Ohari M, Minami T and Osawa Y (1988), "Earthquake Response Analyses of Base Isolation Systems with and without Fail-safe Mechanism," *Proceedings of Ninth World Conference on Earthquake Engineering*, Vol 5, Tokyo-Kyoto, Japan.

PEER NGA Database, Pacific Earthquake Engineering Research Center: NGA database, (http://peer.berkeley.edu/peer_ground_motion_database/).

Skinner RI, Robinson WH and McVerry GH (1993), *An Introduction to Seismic Isolation*, UK: John Wiley & Sons.

Todorovska MI (1999), "Base Isolation by a Soft First Story with Inclined Columns," *Journal of Engineering Mechanics*, **124**(4): 448–457.

Tsai CS, Chiang TC, Chen BJ and Lin SB (2003), "An Advanced Analytical Model for High Damping Rubber Bearings," *Earthquake Engineering and Structural Dynamics*, **32**: 1373–1387.

Warn P and Ryan KL (2012), "A Review of Seismic Isolation for Buildings: Historical Development and Research Needs," *Buildings*, **2**: 300–325.

Wilson EL and Habibullah A (1987), "Static and Dynamic Analysis of Multi-story Buildings Including P-delta Effects," *Earthquake Spectra*, **3**.

Yamada K and Kobari T (2001), "Fundamental Dynamics and Control Strategies for Aseismic Structural Control," *International Journal of Solids and Structures*," **38**(34–35): 6079–6121.